

Microstructure of Al-5Cu-1Li-0.6Mg-0.5Ag-0.5Mn Alloys

Wenzheng Chen ¹, Wenlong Zhang ¹, Dongyan Ding ^{1,*}  and Daihong Xiao ²

¹ School of Materials Science and Engineering, Shanghai Jiao Tong University, Shanghai 200240, China; teddytruck@sjtu.edu.cn (W.C.); zhangwl@sjtu.edu.cn (W.Z.)

² Science and Technology on High Strength Structural Materials Laboratory, Central South University, Changsha 410083, China; daihongx@csu.edu.cn

* Correspondence: dyding@sjtu.edu.cn; Tel.: +86-21-3420-2741

Abstract: Microstructural optimization of Al-Li alloys plays a key role in the adjustment of mechanical properties as well as corrosion behavior. In this work, Al-5Cu-1Li-0.6Mg-0.5Ag-0.5Mn alloy was homogenized at different temperatures and holding times, followed by aging treatment. The microstructure and composition of the homogenized alloys and aged alloys were investigated. There were Al₇Cu₄Li phase, Al₃Li phase, and Al₂CuLi phases in the homogenized alloys. The Al₇Cu₄Li phase was dissolved with an increase in homogenization temperature and holding time. Al₂Cu phase and Al₂CuLi phase coarsened during the homogenization process. The alloy homogenized at 515 °C for 20 h was subjected to a two-stage aging treatment. Peak-age alloy, which had gone through age treatment at 120 °C for 4 h and 180 °C for 6 h, was mainly composed of α-Al, Al₂₀Cu₂Mn₃, Al₂CuLi, Al₂Cu, and Al₃Li phases. Tafel polarization of the peak-age alloys revealed the corrosion potential and corrosion current density to be −779 mV and 2.979 μA/cm², respectively. The over-age alloy had a more positive corrosion potential of −658 mV but presented a higher corrosion current of 6.929 μA/cm².

Keywords: Al-Cu-Li alloys; microstructure; homogenization; aging treatment; corrosion resistance



Citation: Chen, W.; Zhang, W.; Ding, D.; Xiao, D. Microstructure of Al-5Cu-1Li-0.6Mg-0.5Ag-0.5Mn Alloys. *Metals* **2021**, *11*, 37. <https://dx.doi.org/10.3390/met11010037>

Received: 17 November 2020

Accepted: 18 December 2020

Published: 26 December 2020

Publisher's Note: MDPI stays neutral with regard to jurisdictional claims in published maps and institutional affiliations.



Copyright: © 2020 by the authors. Licensee MDPI, Basel, Switzerland. This article is an open access article distributed under the terms and conditions of the Creative Commons Attribution (CC BY) license (<https://creativecommons.org/licenses/by/4.0/>).

1. Introduction

Due to their lightweight, high strength, and hardness, Al-Li alloys have become one of the most potential materials in the aerospace field. Adding 2 wt.% Li can cause the density of aluminum alloys to decrease by 10% while increasing their elasticity modulus by 25–35%. This factor remains unmatched when compared with adding other light elements like Be and Mg [1]. Nevertheless, excessive Li content will cause some negative effects, such as reduced toughness due to excessive precipitation of free-cutting δ'(Al₃Li) phase [2,3], and even enhancing the risk of hydrogen absorption [4]. In contrast to the second-generation Al-Li alloys with over 2 wt.% Li content, the third-generation Al-Li alloys have lower Li and Mg content. The mechanical strength can be improved through alloying with Ag and Zr [5].

Alloying and heat-treatment are effective ways to improve the microstructure and properties of alloys. For example, Wu et al. [6] found that adding Cu not only accelerated the precipitation of the θ'(Al₂Cu) phase and T'(Al₂MgLi) phase but also narrowed the precipitation-free zone. Zheng et al. [7] reported the precipitation sequence of Al-Cu-Li alloys with different Cu content. They found that when the Cu content is above 5 wt.%, the precipitation sequence was GP Zone → θ'' → θ' → θ, and the δ'(Al₃Li) phases would transfer to δ(AlLi) phases. On the other hand, Huang et al. [8] reported the interaction mechanism of adding Mg and Ag elements during phase precipitation. Mg-Ag clusters formed during the aging process and segregation of the clusters could be found on Al {111}_α. At the same time, the interaction of Ag-Li and Cu-Mg could result in the diffusion of Cu and Li toward Mg-Ag clusters, which facilitated the precipitation of the T1 (Al₂CuLi) phase. Eventually, nucleation and growth of T1 (Al₂CuLi) phases could be greatly enhanced [9,10].

Both Zr and Mn could effectively refine the grains. In addition, being different from Mn, Zn could also dissolve into the matrix to form β' (Al_3Zr) phases, which could become the nucleation core of δ' (Al_3Li) phase [11]. According to recent research [12,13], rare-earth elements such as Ce and La could effectively decrease the negative effect caused by Fe and Si and remove the grain boundary weakening effect from Na and K impurities.

Commonly, heat treatment of Al-Li alloys includes homogenization, thermo-mechanical and aging treatment. Homogenization is a method that can greatly reduce the segregation, cavity, and porosity in ingots. Gupta et al. [14] reported that single-homogenization treatment could make low-melting-point compounds precipitate from grain boundaries, which weakened grain boundary strength. However, two-stage homogenization treatment could restrain the precipitation of compounds while preventing over-burning. Pitcher et al. [15] reported that through processing 8091 alloys by two-stage age treatment, pancake structure phases could show up and greatly enhance the mechanical properties of the alloys. Further research [16] reported the strengthening mechanism for two-stage age. During the first-stage aging at a lower temperature, the GP zone (segregation zone of atoms during aging treatment in Al-Cu alloys) showed up and became the nucleation core for precipitation, and several transient phases precipitated along sub-boundaries during the second-stage aging at a higher temperature.

Researchers are exploring the new potential of alloys by alloying specific elements and adjusting the Cu: Li ratio based on the Al-Cu-Li alloy system. The T84 2055 alloys [17,18], developed by Acronix Company (USA), had better static strength. Compared to the third generation alloys, the alloy even had a lower density than other high strength aluminum alloys. To date, few works have been reported on the microstructural evolution and precipitation behavior of Al-Cu-Li alloys with high Cu content, let alone the electrochemical property of the alloys.

Hence, in this study, different homogenization treatment coupled with two-stage age treatment was performed to optimize the microstructure of an Al-Cu-Li-Mg-Ag-Mn alloy. Microstructure evolution and precipitation behavior of the homogenized alloys and aged alloys were investigated. Corrosion behavior of the aged alloys was also studied.

2. Experimental Procedures

The Al-Cu-Li based alloy (Al-5Cu-1Li-0.6Mg-0.5Ag-0.5Mn-0.13Zr-0.1CeLa) were made by vacuum melting. The machined debris of the alloys was tested with DSC (differential scanning calorimetry) of Simultaneous Thermal Analyzer (STA 449 F3, NETZSCH, Selb, Germany) for identifying melting point and optimizing the heating treatment temperature. The heating rate of the DSC test was 10 K/min. After ensuring the suitable homogenization temperature, the ingots were homogenized at different temperatures for different holding times.

The homogenized alloys were hot-extruded to a bar with a diameter of 30 mm. The extruded alloys were solution-treated at 520 °C for 2 h and then quenched by water. The alloy sample of the supersaturated solid solution was put in an electro-thermostatic blast oven (DHG-9075A, Shanghai YiHeng, China) at 120 °C for 4 h, which was the first-stage aging treatment. During the second-stage aging treatment, the samples were aged at 180 °C for different holding times. The hardness of the aged samples was tested with a microhardness tester (400SXV, Shanghai ShangCai, China). The alloy samples were cut into plates and embedded in epoxy resin. The metal surface of the homogenized alloys and the aged alloys were ground with 800, 1000, 2500, 3000, 5000, and 7000 size metallographic sandpapers and polished by polishing clothes. The polishing agent was made up of ethyl alcohol and MgO particles. The precipitation phases of the homogenized alloys and the aged alloys were characterized with a Low Vacuum Ultra-high-resolution Field Emission Scanning Electron Microscope (NOVA nano SEM 230, FEI, Hillsboro, OR, USA) with backscattered SEM detection. Some of the aged alloys were ground into slices with a thickness of 80 μm and thinned by an ion thinning instrument (PIPS 695). The microstructure of the aged alloys was analyzed with a field emission transmission

electron microscope (TALOS F200X, FEI, Hillsboro, OR, USA). The phase composition of the precipitates of the homogenized alloys and the aged alloys were characterized with X-ray diffraction instrument (max 2500, Rigaku D, Japan, Cu target) and EDS (Energy Dispersive Spectrometer) instrument (NOVA nano SEM 230, FEI, Hillsboro, OR, USA).

Electrochemical tests were conducted on an electrochemical workstation (CHI 660E, Shanghai ChenHua, China). To avoid electrochemical test error, three parallel experiments were carried out. All of the aged alloys used 3.5 % NaCl solution as an electrolyte at room temperature with a three-electrode system. The testing range was from -1 V to -0.6 V, and the scan rate was 0.001 V/s. The reference electrode and auxiliary electrode were saturated calomel electrode and platinum, respectively, and the working electrodes were the samples. All potentials were relative to the saturated calomel electrode. The corrosion surfaces were observed with Field-emission Scanning Electron Microscope (Sirion 200, FEI, Hillsboro, OR, USA).

3. Results and Discussion

3.1. As-homogenized Alloys

The alloys were Al-5Cu-1Li alloying with 0.6 wt.% Mg, 0.5 wt.% Ag, 0.5 wt.% Mn, 0.13 wt.% Zr, 0.1 wt.% Ce and La. To determine the optimal homogenization temperature and avoid over-burning, a DSC test was conducted. As shown in Figure 1, the initial melting point was around 520 °C, and the melting point was 620 °C. As a result, the homogenization temperature of our alloy was set at 500 °C and 515 °C, which could decrease the segregation and guarantee that the alloys would not be over-burned.

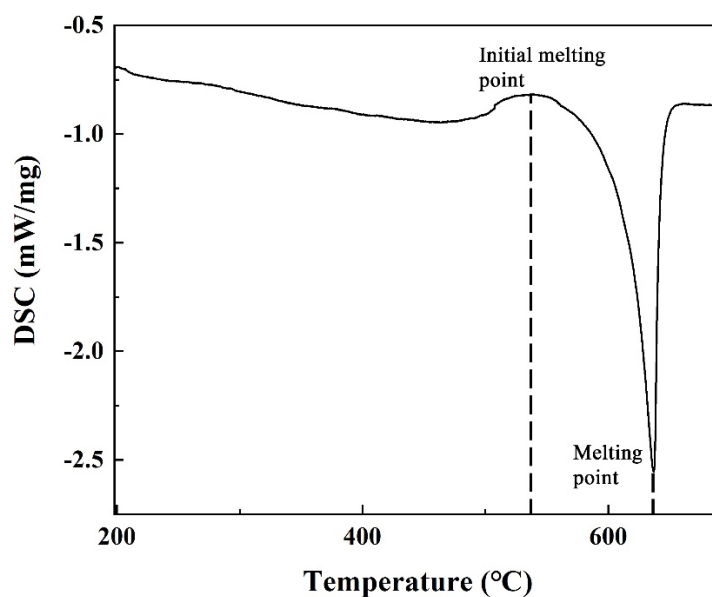


Figure 1. Differential scanning calorimetry (DSC) curve of the alloys.

Figure 2 shows the backscattered SEM images of the homogenized alloys. By comparison, it can be seen from Figure 2a,c that the bone-like phases were smaller and fewer with the increase of the homogenization temperature. Furthermore, with the increase of holding time, bone-like residual phases that precipitated at grain boundaries nearly disappeared, and needle-like precipitates obviously coarsened (Figure 2b,f). Meanwhile, after prolonging the holding time and increasing the homogenization temperature, the distribution density of dot-like particles in Figure 2h was lower than those in Figure 2b. When the homogenization temperature rose to 515 °C, the tabular precipitates show up and coarsen with the increase of holding time (Figure 2h).

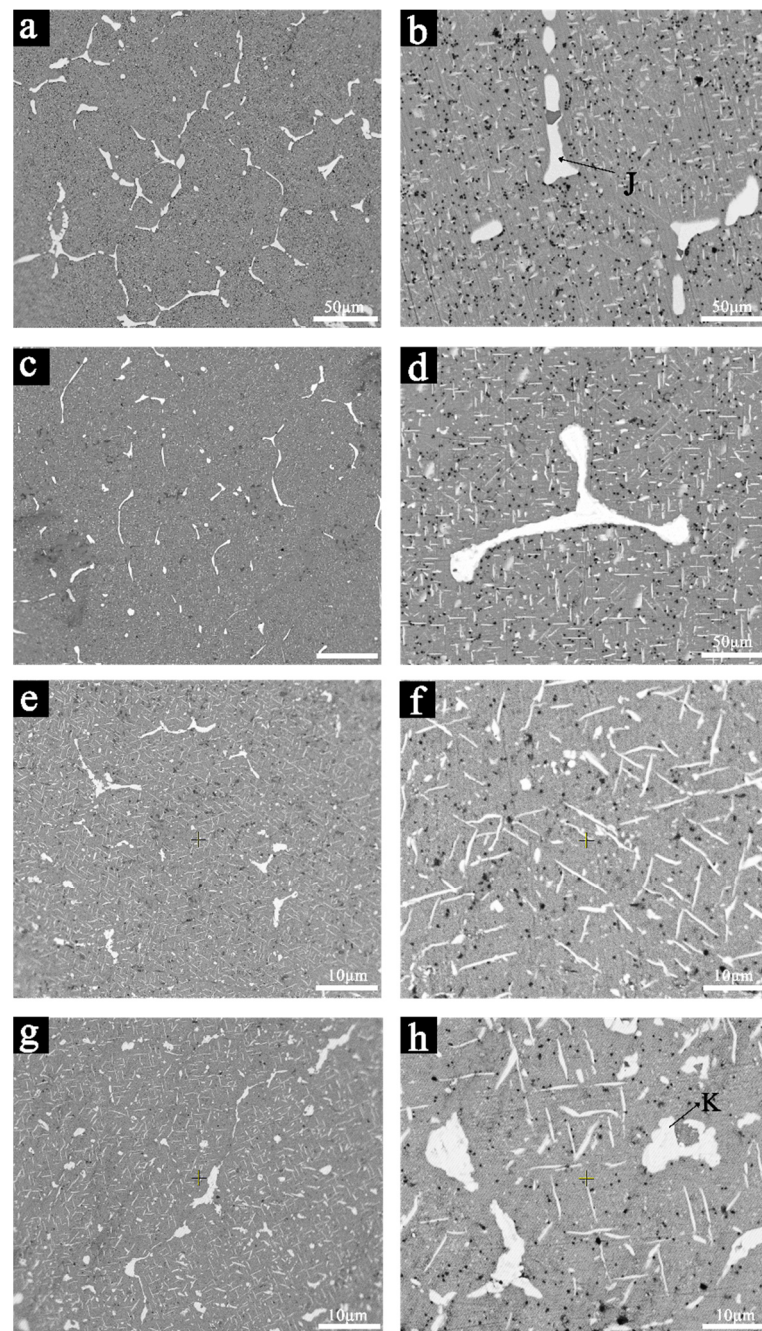


Figure 2. Backscattered SEM images of the as-homogenized alloys: relative low-magnification and microstructure of the alloys as-homogenized at (a,b) 500°C for 8 h, (c,d) 515°C for 8 h, (e,f) 500°C for 20 h, and (g,h) 515°C for 20 h.

XRD patterns of the Al-5Cu-1Li-0.6Mg-0.5Ag-0.5Mn-0.13Zr-0.1CeLa alloy in Figure 3 show that $\text{Al}_7\text{Cu}_4\text{Li}$ phases existed in each sample. The $\text{Al}_7\text{Cu}_4\text{Li}$ phase had a low melting point and usually precipitated along grain boundaries [19], and the peak intensities of $\text{Al}_7\text{Cu}_4\text{Li}$ phase weakened with the increase of homogenization temperature and holding time, which indicated that the content of $\text{Al}_7\text{Cu}_4\text{Li}$ phases decreased. They were dissolved into the matrix during the homogenization treatment. Moreover, according to the recent research and evident morphology features of the second phases [20], the scattered black particles were Al_3Li , and the oriented needle-like precipitates were Al_2CuLi . Table 1 also shows the element composition of marked phases (arrowed by J and K) in Figure 2. It was inferred that the J pointed precipitate was AlCu precipitates. Moreover, according to Chen

et al. [21], research and the morphology of J pointed precipitates, the bone-like precipitates can be identified as AlCuLi precipitates.

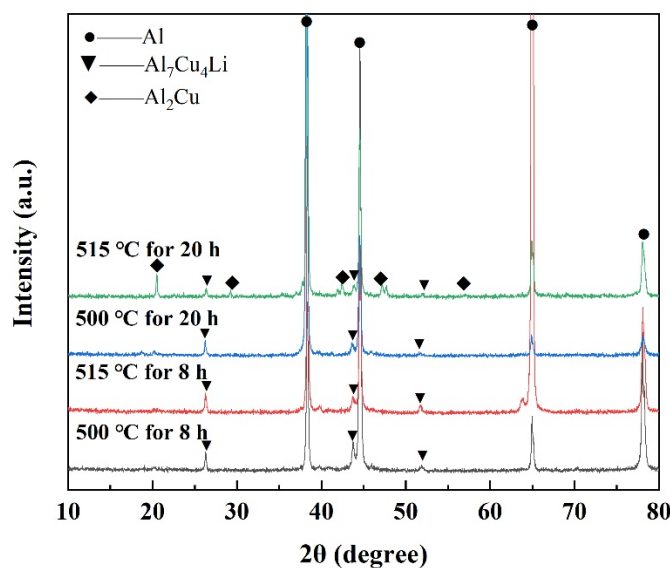


Figure 3. XRD (X-ray diffraction) patterns of the homogenized alloys.

Table 1. Chemical composition of marked phases of homogenized alloys.

| Phases | Mg | Al | Mn | Cu | Zr | Ag | La | Ce |
|----------|------|-------|------|-------|------|------|------|------|
| J, at. % | 0.73 | 69.49 | 0.24 | 29.40 | 0.05 | 0.08 | 0.00 | 0.02 |
| K, at. % | 5.78 | 65.31 | 0.00 | 28.84 | 0.03 | 0.03 | 0.00 | 0.00 |

With the proceeding of homogenization treatment, a phase transition could happen. As shown in Figure 3, Al₂Cu phases were detected in the sample that was homogenized at 515 °C for 20 h. Meanwhile, it was not hard to speculate from the XRD (X-ray diffraction) spectrum in Figure 3 that the growth effect of Al₂Cu phases with the increasing holding time was more prominent when the homogenization temperature was higher. The peaks of Al₂Cu phase were evidently intensified with the extension of holding time when the homogenized temperature was at 515 °C. This phase transition phenomenon can also be found in Figure 2. The particle (K point) showed up when the homogenization temperature rose to 515 °C, and phase precipitation was more distinct as holding times were longer.

In general, Al₇Cu₄Li precipitated along grain boundaries during the casting process. As the homogenization went on, Al₇Cu₄Li was dissolved into the matrix, which resulted in enhanced Cu supersaturation. The higher the homogenization temperature was, or the longer the holding time was, the dissolution of Al₇Cu₄Li was more complete. The undissolved phases, like Al₂CuLi and Al₂Cu, grew up during the homogenization process.

Figures 4–7 present Cu, Ce, and La elemental mapping of the alloys homogenized at different temperatures for different times. It indicated that the Ce and La elements had noticeable segregation. With the increase of homogenizing temperature, the segregation of Ce and La still existed at partial residual phases in Figures 4 and 6. Figures 4b,c and 5b,c show that the segregation of Ce and La elements could not be removed by prolonging the holding time. As shown in Figures 2e and 4b,c, there was no Ce-La segregation where Al₇Cu₄Li phases were located.

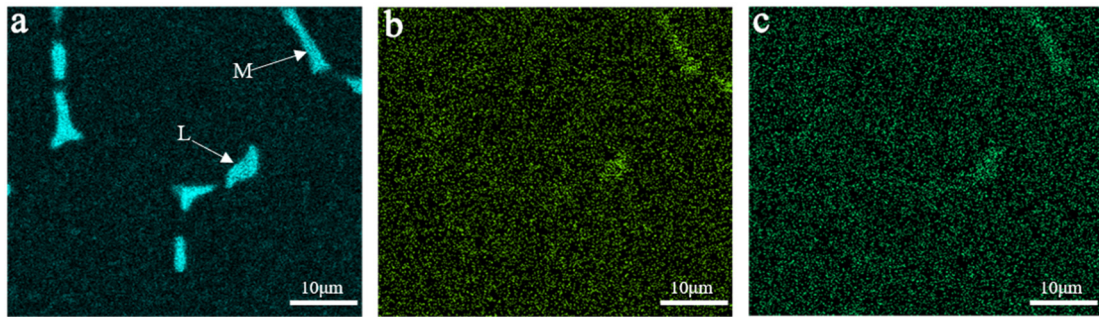


Figure 4. Elemental mapping of the alloy homogenized at 500 °C for 8 h: (a) Cu (Cu-rich precipitates arrowed by L and M), (b) Ce, and (c) La elements.

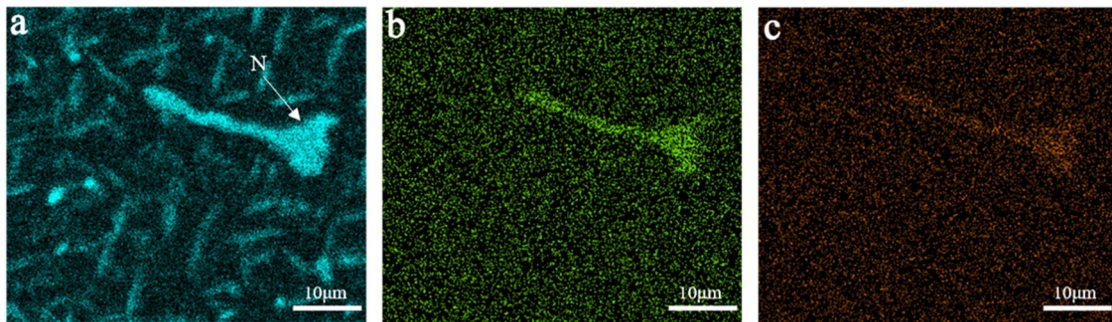


Figure 5. Elemental mapping of the alloy homogenized at 500 °C for 20 h: (a) Cu (Cu-rich precipitate arrowed by N), (b) Ce, and (c) La elements.

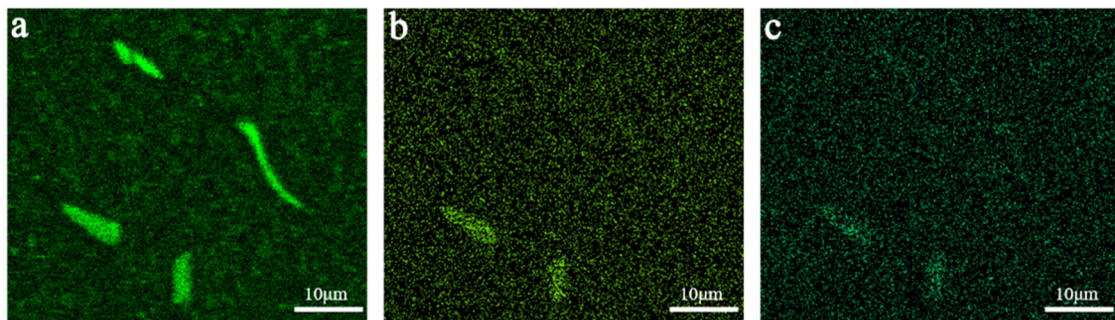


Figure 6. Elemental mapping of the alloy homogenized at 515 °C for 8 h: (a) Cu, (b) Ce, and (c) La elements.

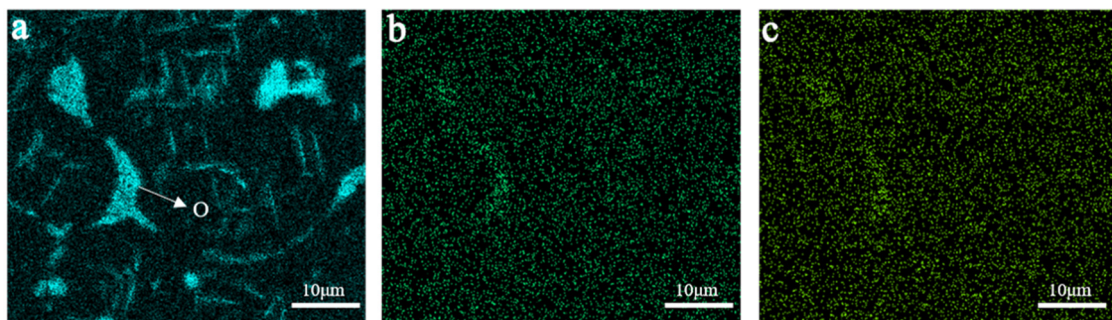


Figure 7. Elemental mapping of the alloy homogenized at 515 °C for 20 h: (a) Cu (Cu-rich precipitates arrowed by O), (b) Ce, and (c) La elements.

Since Mg, Ag, Zr and Mn element were uniformly distributed in the homogenized alloy, the segregation of Ce and La element were exclusively studied as follow. As shown in Figures 4, 5 and 7, the marked particles L, M, N, and O had the Ce and La aggregation.

According to Table 2, the Al:Cu atomic ratio of M, N, and O marked particles was close to 7:2. The marked particle L could be identified as Al_2Cu , since the Al:Cu atomic ratio is 2:1. The Ce-La segregation could be partially found at Al_2Cu of the alloy homogenized at 500 °C for 8 h, but the Ce-La segregation did not exist at the particle (K point in Figure 2h) in the sample homogenized at 515 °C for 20 h.

Table 2. Chemical composition of marked phases in homogenized alloys.

| Phases | Mg | Al | Mn | Cu | Zr | Ag | La | Ce |
|---------|------|-------|------|-------|------|------|------|------|
| L, at.% | 1.32 | 62.68 | 0.15 | 32.53 | 0.53 | 0.13 | 1.21 | 1.45 |
| M, at.% | 1.37 | 75.43 | 0.14 | 20.86 | 0.24 | 0.12 | 0.87 | 0.98 |
| N, at.% | 1.09 | 72.13 | 3.24 | 20.05 | 0.03 | 0.17 | 0.85 | 2.44 |
| O, at.% | 1.81 | 69.97 | 2.56 | 23.42 | 0.00 | 0.19 | 0.77 | 1.28 |

Hence, it can be inferred that the segregation of Ce and La elements tended to form at Cu-rich precipitates, which precipitated at the grain boundaries. The Ce-La elements existed at undissolved precipitates, whose Al:Cu atomic ratio was 7:2, and Al_2Cu phases. With the increase of homogenization temperature and holding time, the segregation of Ce and La elements disappeared from Al_2Cu precipitates.

3.2. Aged Alloys

The alloy homogenized at 515 °C for 20 h were chosen to be solution treated and aged at 120 °C for 4 h and 180 °C for different times. Vickers hardness of aged Al-5Cu-Li-Mg-Ag-Mn alloys is shown in Figure 8. The hardness of the aged alloys increased with an increase in the aging time until it reached the maximum. After the aging time exceeded 6 h, the hardness of aged alloys gradually decreased. Therefore, the peak-age of the alloys could be realized when the alloy was aged at 120 °C for 4 h and then aged at 180 °C for 6 h, and the hardness of the peak-aged alloy was 223 HV of the average value.

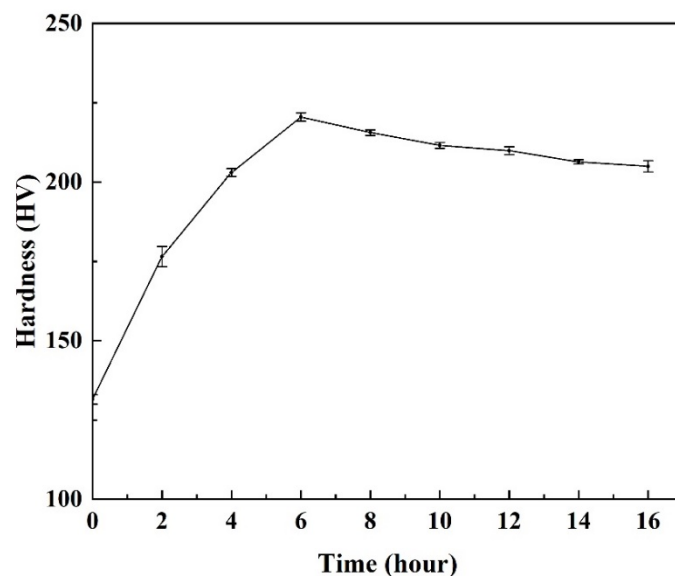


Figure 8. Aging curves of the Al-5Cu-Li-Mg-Ag-Mn alloys.

Microstructure and phase composition of the peak-age alloys was investigated. Backscattered SEM images of the peak-age alloys shown in Figure 9. As shown in Figure 9a, grain boundaries were clear in the backscattered SEM images. The average grain size of the peak-age alloys was close to 30 μm . Compared to the homogenized alloy, there were no needle-like precipitates but scattered bright dot-like particles instead, which can be seen in G area of Figure 9b. The residual phases in the peak-age alloy became smaller. The element composition

of the bright and scattered particles (H point in Figure 9c) was shown in Table 3. It was found that the particle P contains Mn, Cu, and Al elements, so the particle could be identified as Al-CuMn precipitates. Moreover, according to Skolianos et al. [20], the $\text{Al}_{20}\text{Cu}_2\text{Mn}_3$ precipitates existed in Al-Cu-Mn alloy, and the $\text{Al}_{20}\text{Cu}_2\text{Mn}_3$ precipitates were scattered and tiny at the grains. Therefore, it could be inferred that the scattered dot-like particles could be identified as $\text{Al}_{20}\text{Cu}_2\text{Mn}_3$ precipitates. The Al: Cu atomic ratio of Q point was close to 7:2, and we could find the segregation of Mn element at Q point Cu-rich residual phases, according to the composition of Q point of Table 3.

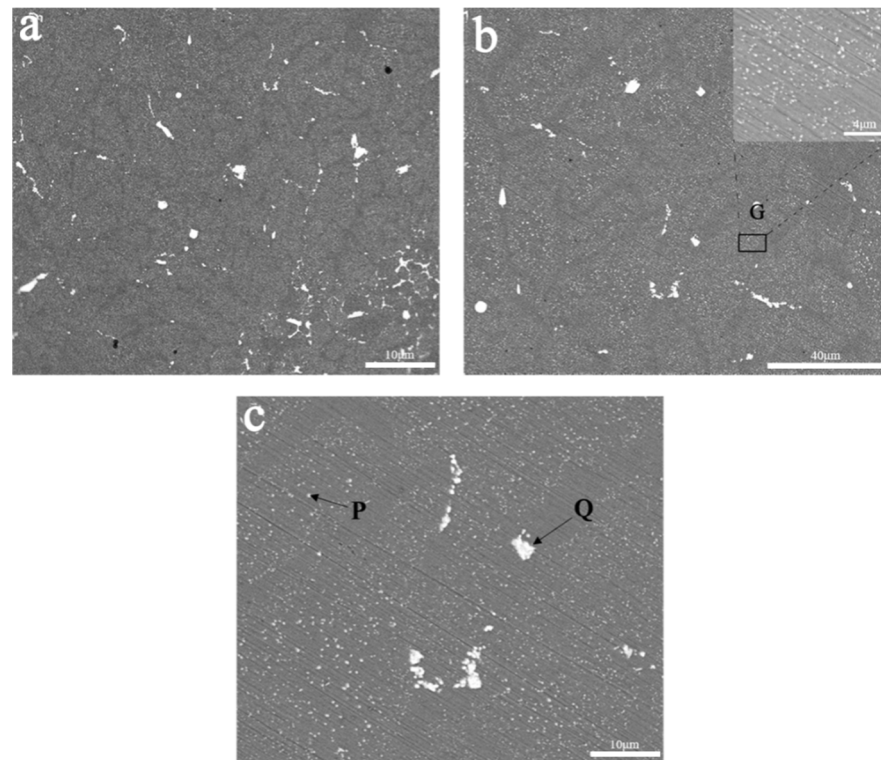


Figure 9. Backscattered SEM images of the aged alloys: (a) grains and precipitates, (b) bright and scattered $\text{Al}_{20}\text{Cu}_2\text{Mn}_3$ precipitates (high magnification image of scattered $\text{Al}_{20}\text{Cu}_2\text{Mn}_3$ in area G), and (c) residual precipitates arrowed by Q and scattered $\text{Al}_{20}\text{Cu}_2\text{Mn}_3$ precipitates arrowed by P.

Table 3. Chemical composition of marked phases in the peak-age alloys.

| Point | Mg | Al | Mn | Cu | Zr | Ag | La | Ce |
|---------|------|-------|------|-------|------|------|------|------|
| P, wt.% | 0.79 | 84.76 | 7.03 | 6.79 | 0.33 | 0.30 | 0.00 | 0.00 |
| Q, wt.% | 0.78 | 68.62 | 6.70 | 19.26 | 0.37 | 0.36 | 2.79 | 1.13 |

Figure 10 also shows element mapping of the aged alloys. It could be found that element distributions of Mg, Ag, and Zr were uniform, but Ce and La segregations still existed, according to the Ce and La contents of Q point spot scan in Table 3. Compared to the homogenized alloys, segregation of Mn element became distinct after aging treatment, which could prove that $\text{Al}_{20}\text{Cu}_2\text{Mn}_3$ tends to precipitate at the Cu-rich residual phase. After extrusion, the dislocations were generated and entangled, forming lineage boundaries, which could become nucleation point of phase precipitation [22]. Moreover, alloying with Mg, Ag, Zr, and Mn could make precipitates become smaller and more scattered [8,23].

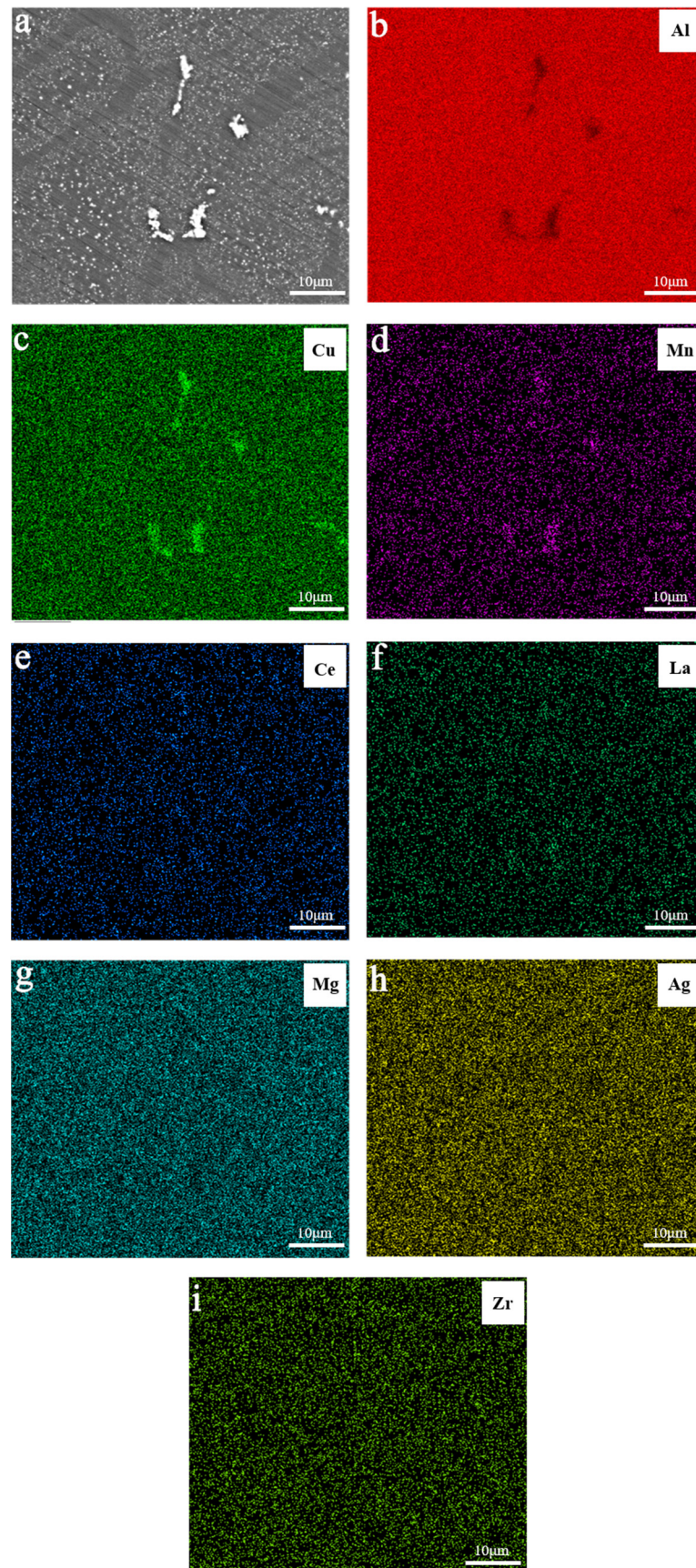


Figure 10. (a) Backscattered SEM images and elemental mapping images of the aged alloys: (b) Al, (c) Cu, (d) Mn, (e) Ce, (f) La, (g) Mg, (h) Ag, m and (i) Zr elements.

Figure 11 present TEM (Transmission Electron Microscope) images of the aged alloy in which $\text{Al}_{20}\text{Cu}_2\text{Mn}_3$ precipitates were observed as well as T1 (Al_2CuLi), δ' (Al_3Li) and θ' (Al_2Cu). The average diameter of the $\text{Al}_{20}\text{Cu}_2\text{Mn}_3$ phases was around $0.3 \mu\text{m}$. Dispersed distribution of $\text{Al}_{20}\text{Cu}_2\text{Mn}_3$ particles was attributed to alloying with Mn element. Skolianos et al. [20] reported that scattered $\text{Al}_{20}\text{Cu}_2\text{Mn}_3$ precipitates in Al-4.5Cu-2.0Mn alloy could become the nucleation point of recrystallization. Therefore, the recrystallized grain became fine.

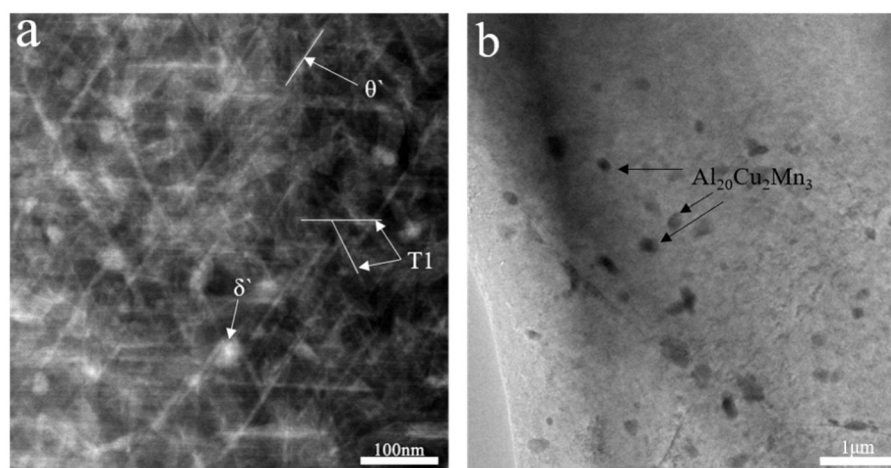


Figure 11. TEM (Transmission Electron Microscope) images of the aged alloy: microstructural morphology of (a) nano-scale precipitates of θ' , T1 and δ' , and (b) $\text{Al}_{20}\text{Cu}_2\text{Mn}_3$ phase in the aged alloys.

According to Wang et al. [24], the T1 (Al_2CuLi) phases precipitated along $\{111\}_\alpha$, and θ' (Al_2Cu) precipitated along $\{100\}_\alpha$. The T1 (Al_2CuLi) phases had an orientation relationship with α -Al of $(0001)\text{T1} // \{111\}_\alpha$ and $\langle 10\bar{1}0 \rangle // \langle \bar{1}10 \rangle$. Figure 11a shows TEM image of the aged alloys recorded along $\langle 110 \rangle$. The T1 (Al_2CuLi) precipitates in Figure 11, presented as needle-like precipitates, and the Al_2Cu precipitates were the same. Meanwhile, according to Kilmer et al. [25], the bright particles in Figure 11a were δ' (Al_3Li) phase, which was much smaller than $\text{Al}_{20}\text{Cu}_2\text{Mn}_3$ particles shown in Figure 11b. The T1 (Al_2CuLi) precipitates were attributed to alloying with Mg and Ag elements [26]. Mg-Ag clusters diffused toward GP zone along $\{111\}_\alpha$ during the first aging treatment, and at the second aging treatment, the Li and Cu elements diffused toward the GP zone due to the interaction between Ag-Li and Mg-Cu [8]. Hence, the nucleation and growth of the T1 (Al_2CuLi) phase could be realized during the two-stage aging treatment. T1 (Al_2CuLi) precipitate could make the dislocation bend when the dislocation passed by the T1 (Al_2CuLi) hard phase. In this case, the T1 (Al_2CuLi) phase could greatly restrain the movement of dislocation and produce dislocation tangling, and thus strengthen the alloys [24].

3.3. Corrosion Performance

Figure 12 showed typical Tafel curves of the peak-age alloy and over-age alloy, which was first aged at 120°C for 4 h and then aged at 180°C for 16 h. Tafel polarization parameters are shown in Table 4. E_{corr} represents the corrosion potential of alloy corrosion, and I_{corr} represents corrosion current density. It could be found from Figure 12 that the Tafel curves of different aged alloys were typical Tafel curves of aluminum alloys. The higher E_{corr} was, the alloys were more difficult to be corroded [27]. The Tafel polarization parameters in Table 4 revealed that E_{corr} of the aged alloys increased with the increase of the second stage aging time. It could be inferred that the over-aged alloys were more difficult to be corroded than the peak-aged alloys. However, the over-aged alloys also have higher I_{corr} , which indicated that the corrosion of the over-age alloys in 3.5% NaCl solution was faster than that of the peak-aged alloys.

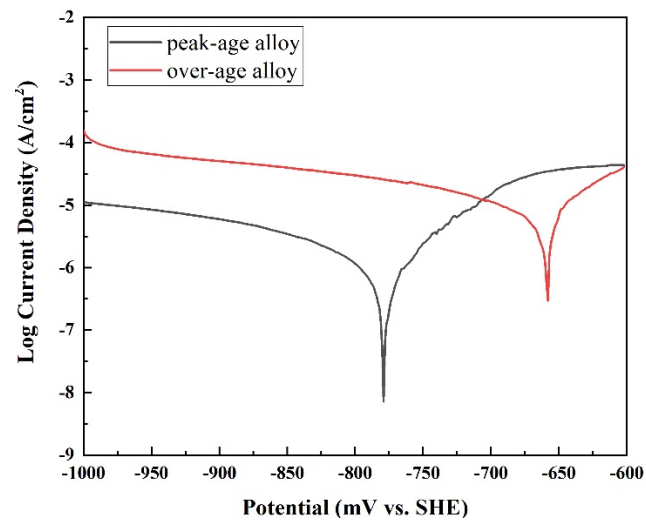


Figure 12. Typical Tafel polarization curve of the peak-age alloy and over-age alloy.

Table 4. Tafel polarization parameters of the aged Al-Li alloys tested in 3.5% NaCl solution.

| Alloy | E_{corr} (mV vs. SCE) | I_{corr} ($\mu\text{A}/\text{cm}^2$) |
|----------|--------------------------------|---|
| Peak-age | −779 | 2.979 |
| Over-age | −658 | 6.929 |

E_{corr} : corrosion potential of alloy corrosion; I_{corr} : corrosion current density.

The corrosion surfaces of the aged alloys tested after Tafel tests were shown in Figure 13. The aged alloys presented pitting corrosion. However, comparing Figure 13a,b, there was difference in the number of corrosion pits for different aging treatments. The over-age alloys showed more corrosion pits than those of the peak-age alloys. Meanwhile, Figure 14a,b also show the high-magnification images of corrosion pits of the peak-age alloy and the over-age alloy. The corrosion pit of the over-age alloy was much bigger than that of the peak-age alloy. The number of corrosion pits and the size of the pit could reflect the degree of corrosion. Therefore, the corrosion became more severe, which was consistent with the Tafel curves and Tafel polarization parameters. Commonly, the bigger the second phase was, the more severe the corrosion was [28]. Consequently, the severe corrosion of the over-aged alloy also reflected the bigger second phases in the over-aged alloy.

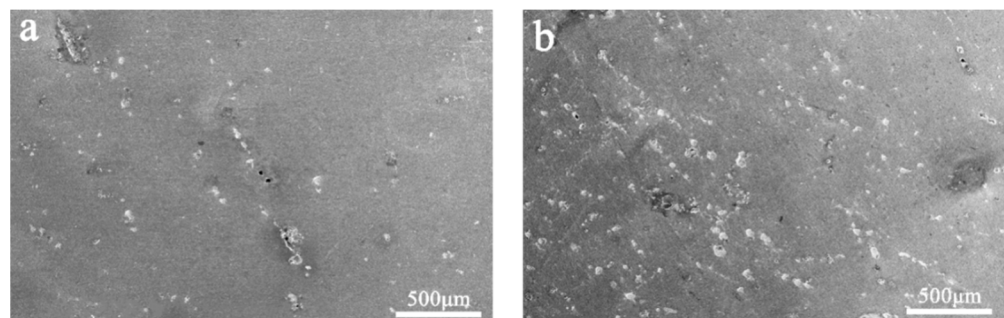


Figure 13. Corrosion surfaces of the alloy tested in 3.5% NaCl solution: (a) peak-age alloy and (b) over-age alloy.

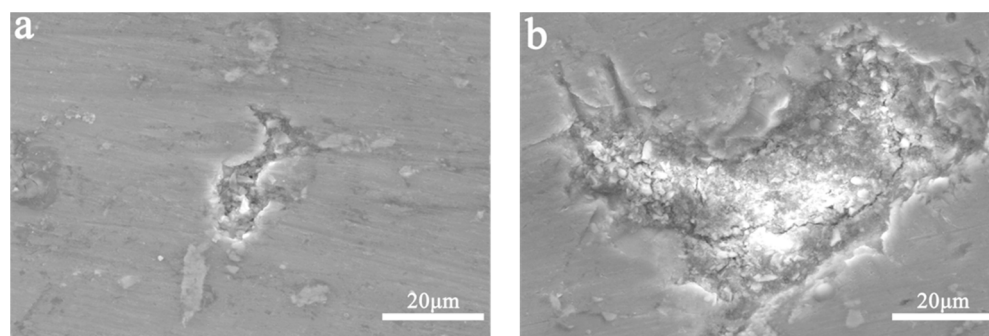


Figure 14. Corrosion pits of the alloy tested in 3.5% NaCl solution: (a) peak-age and (b) over-aged alloys.

4. Conclusions

The Al-5Cu-1Li-0.6Mg-0.5Ag-0.5Mn alloys with Zr, Ce, and La elements should be homogenized at a temperature lower than 520 °C to avoid over-burning. Due to the high content of Cu element, the phase precipitation during the homogenization treatment was abundant and dispersed. Al₇Cu₄Li, Al₂Cu, Al₃Li, and Al₂CuLi were the main phases in the homogenized alloys. With an increase of homogenization temperature and holding time, the Al₇Cu₄Li phases were gradually dissolved, and Al₂Cu phases and Al₂CuLi grew up. The growth rate of the Al₂Cu precipitates was remarkably increased after the homogenization temperature increased from 500 °C to 515 °C. Moreover, the Ce and La segregations were found in the Cu-rich precipitates.

After extrusion, solution treatment, and two-stage age treatment, the mechanical property was greatly enhanced. Peak-age could occur after the alloy was aged at 120 °C for 4 h and then aged at 180 °C for 6 h. The hardness of the peak-age alloy was 223 HV. The precipitation of the aged alloys was more scattered and uniform in comparison with that of the homogenized alloys. The Al₂₀Cu₂Mn₃ precipitates were distributed in the matrix, and Cu-rich particles mainly precipitated along grain boundaries. Moreover, the Al₂CuLi, Al₂Cu, and Al₃Li phases existed in the aged alloy. The typical Tafel testing showed that the corrosion resistance effect could be enhanced with an increase of the aging time, but the over-aged alloys presented a higher corrosion speed.

Author Contributions: Conceptualization, D.D.; formal analysis, W.C., D.X.; investigation, W.C., W.Z.; writing—original draft preparation, W.C.; writing—review and editing, W.C. and D.D.; project administration, D.D. All authors have read and agreed to the published version of the manuscript.

Funding: This work was supported by the Open Research Fund (No. ZN2019006) of Science and Technology on High Strength Structural Materials Laboratory, Central South University, China.

Acknowledgments: The authors would like to thank the Instrumental Analysis Center of Shanghai Jiaotong University for SEM experiments.

Conflicts of Interest: The authors declare no conflict of interest.

References

1. Ali, A.E.; Xu, Y.; Zhang, S.H.; Ma, Y.; Chen, D.Y. 1420, 8090 and 2060 Al-Li alloys sheet undergoing different strain rates and fibre orientation. *Proc. Eng.* **2017**, *207*, 13–18.
2. Zakharov, V.V. Some problems of the use of aluminum-lithium alloys. *Met. Sci. Heat Treat.* **2003**, *45*, 49–53. [[CrossRef](#)]
3. Ber, L.B.; Vainblat, Y.M. A study of the nature of structural hardening and anisotropy of the yield strength of alloy D16. *Metall. Cast. Light Alloys.* **1977**, 147–164.
4. Bennett, C.G.; Lynch, S.P. Fracture toughness of 2090 Al-Li-Cu extrusions with high and low hydrogen contents. *Mater. Sci. Eng. A* **1998**, *247*, 32–39. [[CrossRef](#)]
5. Rioja, R.J. Fabrication methods to manufacture isotropic Al-Li alloys and products for space and aerospace applications. *Mater. Sci. Eng. A* **1998**, *257*, 100–107. [[CrossRef](#)]
6. Wu, L.; Li, Y.G.; Li, X.F.; Ma, N.H.; Wang, H.W. Interaction between cadmium and multiple precipitates in and Al-Li-Cu alloy: Improving aging kinetics and precipitation hardening. *J. Mater. Sci. Technol.* **2020**, *46*, 44–49. [[CrossRef](#)]

7. Zheng, Z.Q.; Zhang, W.B.; Cui, Q. Aluminum-lithium alloy for the aerospace industry. *Mater. Sci. Eng. A* **1990**, *8*, 20–25.
8. Huang, B.P.; Zheng, Z.Q. Independent and combined roles of trace Mg and Ag additions in properties precipitation process and precipitation kinetics of Al-Cu-Li-(Mg)-(Ag)-Zr-Ti alloys. *Acta Mater.* **1998**, *46*, 4381–4393. [[CrossRef](#)]
9. Medjahed, A.; Moula, H.; Zegaouia, A. Influence of the rolling direction on the microstructure, mechanical, anisotropy and gamma rays shielding properties of an Al-Cu-Li-Mg-X alloy. *Mater. Sci. Eng. A* **2018**, *732*, 129–137. [[CrossRef](#)]
10. Examilioti, T.N.; Klusemann, B.; Kashaev, N. Anisotropy and size effect in tensile mechanical properties of Al-Cu-Li 2198 alloy. *Proc. Struct. Integr.* **2017**, *5*, 13–18. [[CrossRef](#)]
11. Wang, Y.; Wu, H.J.; Liu, X.T.; Jiao, Y.L. High-strength and ductility bimodal-grained Al-Li/Al-Li-Zr composite produced by accumulative roll bonding. *Mater. Sci. Eng. A* **2019**, *761*, 138049. [[CrossRef](#)]
12. Nazarov, S.; Rossi, S.; Bison, P. Influence of rare earths addition on the properties of Al-Li alloys. *Phys. Met. Metall.* **2019**, *120*, 402–409. [[CrossRef](#)]
13. Meng, L.; Zheng, X.L. Overview of the effects of impurities and rare earth elements in Al-Li alloys. *Mater. Sci. Eng. A* **1997**, *237*, 109–118. [[CrossRef](#)]
14. Gupta, R.K.; Nayan, N.; Nagasireesha, G. Development and characterization of Al-Li alloys. *Mater. Sci. Eng. A* **2006**, *420*, 228–234. [[CrossRef](#)]
15. Pitcher, P.D. Aging of forged aluminum-lithium 8091 alloy. *Scripta Metall.* **1988**, *22*, 1301–1306. [[CrossRef](#)]
16. Cina, B.; Ranish, B. New technique for reducing susceptibility to stress corrosion of high strength aluminum alloys. *Al. Ind. Prod.* **1974**, *27*, 79–84.
17. Rioja, R.J.; Liu, J. The evolution of Al-Li base products for aerospace and space applications. *Metall. Mater. Trans. A* **2012**, *43*, 3325–3337. [[CrossRef](#)]
18. Fridlyander, I.N. Aluminum alloys in aircraft in the period of 1970 – 2000 and 2001 – 2015. *Met. Sci. Heat Treat.* **2001**, *43*, 6–10. [[CrossRef](#)]
19. Luo, L.; Luo, L.S.; Li, Z.P.; Su, Y.Q. Microstructural evolution of Al-Cu-Li alloys with different Li contents by coupling of near-rapid solidification and two-stage homogenization treatment. *Chin. Found. Res. Develop.* **2020**, *17*, 190–197. [[CrossRef](#)]
20. Skolianos, S.M.; Katramis, T.Z.; Devereux, O.F. Microstructure and corrosion behavior of as-cast and heat-treated Al-4.5Cu-2.0Mn alloys. *Metall. Trans. A* **1989**, *20*, 2499–2516. [[CrossRef](#)]
21. Chen, A.; Peng, Y.; Zhang, L. Microstructural evolution and mechanical properties of cast Al-3Li-1.5Cu-0.2Zr alloy during heat treatment. *Mater. Charact.* **2016**, *11*, 234–242. [[CrossRef](#)]
22. El-Aty, A.A.; Xu, Y.; Guo, X.Z.; Zhang, S.H. Strengthening mechanisms, deformation behavior, and anisotropic mechanical properties of Al-Li alloys: A review. *J. Adv. Res.* **2018**, *10*, 49–67. [[CrossRef](#)] [[PubMed](#)]
23. Zheng, Z.Q.; Zhao, Y.Q.; Liu, M.G.; Yin, D.F. The microstructure and fracture toughness of an Al-Li-Cu-Mg-Zr alloy containing minor lanthanum additions. *Mater. Sci. Lett.* **1994**, *13*, 946–949. [[CrossRef](#)]
24. Wang, X.M.; Shao, W.Z.; Jiang, J.T.; Li, G.A.; Wang, X.Y. Quantitative analysis of the influences of pre-treatments on the microstructure evolution and mechanical properties during artificial age of an Al-Cu-Li-Mg-Ag alloy. *Mater. Sci. Eng. A* **2020**, *782*, 139253. [[CrossRef](#)]
25. Kilmer, R.J.; Stoner, G.E. Effect of Zn additions on precipitation during age of alloy 8090. *Scripta Mater.* **1991**, *25*, 243–248. [[CrossRef](#)]
26. Hirosawa, S.; Sato, T.; Kamio, A. Effects of Mg addition on the kinetics of low-temperature precipitation in Al-Li-Cu-Ag-Zr alloys. *Mater. Sci. Eng. A* **1998**, *242*, 195–201. [[CrossRef](#)]
27. Sauvage, X.; Bobruk, E.V.; Murashkin, M.Y.; Nasedkina, Y.N.; Enikeev, A.R.; Valiev, Z. Optimization of electrical conductivity and strength combination by structure design at the nanoscale in Al-Mg-Si alloys. *Acta Mater.* **2015**, *98*, 355–366. [[CrossRef](#)]
28. Ralston, K.D.; Fabijanic, D.; Birbilis, N. Effect of grain size on corrosion of high purity aluminium. *Electrochim. Acta* **2011**, *56*, 1729–1736. [[CrossRef](#)]